

Chapter 2

Understanding GPR via a Simulator

GPR radargrams often have no resemblance to the subsurface structures over which the profile was recorded. Various factors including the innate design of the survey equipment and the complexity of electromagnetic propagation in the ground can disguise complex near surface earth structures recorded on GPR reflection profiles. A very useful way to understand the nature and content of GPR radargrams is to understand what components are needed to develop a basic simulator. The simulator would provide a means to predict radargrams made across candidate models of the ground and help to explain how buried target structures get translated into recorded reflection profiles. The simulator can show the limitations of this remote sensing method, but also highlight the capabilities of GPR and where this exploration tool and in what subsurface environments that it can and cannot function optimally.

The main components required to build a simulator for GPR would include design elements for creating an electromagnetic model of the ground. The simulator has to incorporate the theory on how electromagnetic radar waves will propagate in the model created, and it must also account for the engineering design of the simulated GPR equipment that is used to estimate recorded reflections made over the model. The following basic list of items need to be defined and built into the simulator and include:

- Earth Model
- Reflection
- Transmission
- Refraction
- Attenuation
- Antenna Beam
- Antenna Pulse
- Raypaths

Some of these components in the simulator we either have to define, such as the earth model, or things that we need to know about the basic propagation of radar waves, such as how they reflect, transmit or refract, as well as attenuate in ground.

Other things required in the simulator include knowledge about the equipment being used such as the directional response of the antenna beam as well as the pulse shape of the burst of microwave energy transmitted into the ground. All of these components will have to be described or set and programmed into the simulator before a synthetic radargram can be generated across a model structure of the ground.

Each one of these essential components used in the simulator is discussed in more detail and descriptions drawn to help understand the transmission of microwave into the ground and the final recording of the radar waves. The list above is by no means meant to be complete as the “true” propagation of radar waves predicted by any simulator is just an approximation of the real world propagation (Giannopoulos 2005, Powers and Olhoeft 1995). Predicting radargrams over model structures, as is common in geophysical forward modeling, can greatly assist in understanding the complex nature of GPR signals recorded on even the simplest of subsurface structures. Understanding the complex radar patterns can help interpreters in the diagnosis of GPR radargrams and from falling into interpretive pitfalls. Learning about the simulation of GPR will more than likely place breaks on nonchalant interpretations made about reflections observed on raw radargrams.

2.1 Earth Model

One way to consider the near surface ground is that it is comprised of capacitors and wires, where different materials and soils have different sized capacitors and wires (Fig. 2.1). The capacitor or dielectric relates to the ability of the ground to store charge. The larger the dielectric the more charge that can be stored in ground. If the ground can store charges while a microwave transmits through it, then dielectrics will act to impede the microwave from penetrating very quickly into the ground at depth since the ground is acting to store the microwave and charge the ground along the way. On the other hand, when a material or soil has weak or non-existent dielectric properties, there is essentially no impediment to the travel of the microwaves. Microwaves traveling through low dielectric material will travel faster, approaching the speed of light in a vacuum when the dielectric is 1.

The velocity of microwaves for a material as a function of its dielectric and conductivity is given by (Cassidy, 2009):

$$v(f) = \frac{C}{\sqrt{\epsilon'(f)\mu_r \frac{1+\sqrt{1+\tan^2\delta}}{2}}} \quad (2.1)$$

where the loss tangent



Fig. 2.1 A schematic diagram indicating an idealized ground which is composed of varying dielectric material and of wires having varying conductivity

$$\delta = \frac{\varepsilon'' + \frac{\sigma_{dc}}{2\pi f \varepsilon_0}}{\varepsilon'(f)} \quad (2.2)$$

and ε' is the real dielectric, ε'' is the complex dielectric, σ_{dc} the conductivity, f is the frequency, C is the speed of light, ε_0 is the permittivity of free space, and μ is the magnetic permeability. This equation for the velocity of microwaves indicates that they are a function of frequency. In general, if the loss tangent is small, and the velocity of microwaves is not a strong function of frequency, which is generally the case for microwave in the range 10 MHz–1 GHz, then this equation reduces to a familiar form:

$$v = \frac{C}{\sqrt{\varepsilon}} \quad (2.3)$$

The velocity of a material is inversely related to the square root of its dielectric in the simplest form. The dielectric of a vacuum is 1 (which is also close to the dielectric of air) – and the velocity of light in air is the speed of light. Interestingly, one of the slowest materials for microwaves to travel in is water, which has a dielectric of 81. Microwaves that travel through water have a velocity that is 1/9th the speed of microwaves in air. Most earth materials (see Table 2.1) have dielectrics that vary between 5 and 35. Conductivities of varying soil materials also have a wide dispersion since the conductivity drastically changes by any inclusion of water or moisture into the soil.

Table 2.1 Typical (approximated) values of conductivity and real dielectric found for some materials (adapted after Daniels 1996, 2004; Ulriksen 1982). The values of velocity, wavelength and attenuation are based on a 400 MHz microwave. (Electrical properties are shown to be quite variable between dry and wet conditions.)

Material	E real	Conductivity mho/m	Velocity cm/ns	Wavelength cm	Attenuation 1/m
air	1	0	30	75	0
asphalt	6	.001	12.25	30.62	0.08
basalt	8	.01	10.6	26.51	0.67
clay (wet)	12	.1	8.52	21.29	5.35
concrete	7	.0001	11.34	28.35	0.01
copper	1	5.8	2.62	6.55	95.52
granite	5	1E-8	13.42	33.54	0
sandstone (wet)	6	.04	12.11	30.29	3.04
soil-loamy (dry)	2.5	.00011	18.97	47.43	0.01
soil-loamy (wet)	19	.021	6.88	17.2	0.91
soil-sandy (dry)	2.5	.00014	18.97	47.43	0.02
soil-sandy (wet)	25	.007	6	15	0.26
soil-clayey (dry)	2.4	.0003	19.36	48.41	0.04
soil-clayey (wet)	15	.05	7.72	19.31	2.43
silicon	12	.001	8.66	21.65	0.05
sand (dry)	9	.001	10	25	0.06
snow	1.4	.0000001	25.35	63.39	0
water	81	.01	3.33	8.33	0.21
water (pure)	81	.0001	3.33	8.33	0
water (salt)	81	4	2.54	6.36	63.91
freshwater-ice	4	.001	15	37.5	0.09
permafrost	8	.001	10.61	26.52	0.07
iron	1	1000000	0.01	0.02	39738.35
wood (dry)	3	.003	17.32	43.29	0.33
sand	8	.003	10.61	26.52	0.2

The first step in the model construction is to define all the electrical properties of the materials and boundaries that are to be included in the simulation. This essentially requires defining the dielectric and the conductivities for the different structural elements in the subsurface. These material properties are set through a digitized grid that also stores the slopes and lines of structural boundaries. Of course the real earth model can have infinitely variable dielectrics and conductivities located at all the locations in the ground and this is impossible to completely set. However, for many earth models with only several distinct structures, reasonable estimates of the homogenous elements in this model can be defined in a discrete and

digitized grid. For the subsurface structures studied, digitizing the earth model around 1 cm or less can adequately be used for mapping the reflection/transmission of GPR microwaves for most of the mid-range antenna frequencies from 100 to 800 MHz used in archaeology.

2.2 Reflection

Once the model candidates are determined and boundaries drawn to describe the subsurface model structures, the next step is to program how microwaves will reflect off these features. The ratio of reflected amplitude to the incident amplitude, described by the reflection coefficient for microwaves (with parallel polarization) between a material 1 and material 2 is given by:

$$R = \frac{Z_2 \cos \theta_1 - Z_1 \cos \theta_2}{Z_2 \cos \theta_1 + Z_1 \cos \theta_2} \quad (2.4)$$

(after Annan 2009) where the complex electromagnetic impedance Z is given by

$$Z = \sqrt{\frac{j\omega\mu}{\sigma + j\omega\epsilon}} \quad (2.5)$$

and θ_1 the angle of incidence and θ_2 the angle of refraction of the transmitted wave (discussed in a later section), and j the imaginary number. It is useful to understand the reflection equation for vertical incidence of the radar wave. The reflection of microwaves for vertical incidence is given by:

$$R = \frac{Z_2 - Z_1}{Z_2 + Z_1} \quad (2.6)$$

Equation 2.6 is also sometimes written for the case when conductivity is negligible to

$$R = \frac{\sqrt{\epsilon_1} - \sqrt{\epsilon_2}}{\sqrt{\epsilon_1} + \sqrt{\epsilon_2}} \quad (2.7)$$

Equation 2.7 states that the reflection strength is related to the difference between the square roots of the dielectric between the materials. This is an important descriptor of how much energy is reflected by radar waves off of subsurface objects. The amount of reflection is related to the difference between the electrical parameters, primarily the dielectric of the materials. If there is no contrast buried in the ground – there is no reflection! This equation also tells us that GPR does not generate unique reflection strengths. The method at best can measure the degree of electrical contrast that is present at the boundary between two materials where a reflection occurred. GPR cannot uniquely define a material simply based on the

strength of the reflection – GPR is not a “gold” finder per se, but better said a “contrast” finder. With Eqs. 2.4, 2.5, 2.6 and 2.7, the strength of the radar wave reflecting from any subsurface structures that are made in our model earth can easily be calculated. For an example of two materials where the conductivities are negligible and where the dielectrics are $\epsilon_1=9$ and $\epsilon_2=16$, about 1/7th of the initial amplitude would get reflected at the boundary. In another example, if one is considering the reflection from a buried metallic object (conductivity 10,000 mho/m for iron as an example) in contact with a soil (conductivity 0.01 mho/m), we must consider the conductivity in Eq. 2.7. In this case, the reflection field strength gives a value of 0.9999 or nearly all the microwave is reflected from the metal object!

Another interesting observation that can be surmised from Eq. 2.7 is that the reflection amplitude can change sign depending on the which dielectric is larger or smaller. When the reflection amplitude is negative the wave will invert on reflection. These are commonly called phase reversals and are often discernible in many real situations.

As the wave travels in the ground it may encounter many other subsurface features that it will need to reflect off of. The simulator software continually monitors the wave at each boundary as multiple reflections are made. The strength of the reflection as it is diminished by multiple reflections within the model earth are stored as the wave travels through the grid.

2.3 Transmission

The transmission of radar waves for parallel polarization at an interface between two materials is given by the equation

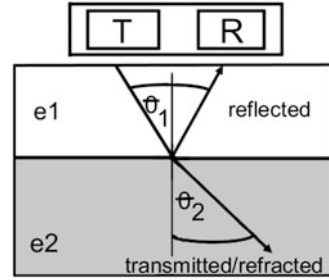
$$T = \frac{2Z_2 \cos \theta_1}{Z_2 \cos \theta_1 + Z_1 \cos \theta_2} \quad (2.8)$$

For vertical incidence this equation reduces to:

$$T = \frac{2Z_2}{Z_2 + Z_1} \quad (2.9)$$

In the case of a wave encountering a metal target on its path at normal incidence, the transmission into the boundary is nearly 0 since the impedance Z_2 which is proportional to the inverse square root of the conductivity is close to 0 for large conductivity. The other way to look at the problem is that since nearly all the energy is reflected off the boundary of a metal object, then there is no transmission of any significant energy into the metal object. Thus GPR cannot look through metal – it can only see the top of metal!

Fig. 2.2 The reflection and transmission of a microwave at a boundary where electrical contrast exists between two materials



In the case of negligible conductivity for both materials Eq. 2.9 can be reduced to the special case

$$T = \frac{2\sqrt{e_1}}{\sqrt{e_1} + \sqrt{e_2}} \quad (2.10)$$

When the dielectrics of two materials are the same then there is no reflected wave and the transmitted wave is unity assuming the conductivities are also the same.

2.4 Refraction

The microwave that transmits across an anomalous structure will refract – e.g. change its direction. The new angle that the transmitted wave will refract to at a boundary is given by an ancient – archaeological formula – Snell's Law:

$$\frac{\sin \theta_1}{\sin \theta_2} = \frac{v_1}{v_2} \quad (2.11)$$

Examination of Snell's Law indicates that the larger the contrast in velocity (or the electrical contrast) between two materials – the larger the change in the angle the refracted wave will have from its incident wave (Fig. 2.2).

A good way to visualize refraction is to make an idealized earth model and a simple radar antenna where all the waves are radiating out in a cone from the antenna. The refraction of microwaves for a simplified earth model where just the dielectric is getting smaller with depth – e.g. the velocity is getting faster with depth – is shown in the *top* diagram of Fig. 2.3. Here, the transmitted waves are shown to be refracting away from the vertical-downward direction. Transmission into higher velocity media causes the refraction of the waves and makes the beam appear much broader with increasing depth. With the broadening beam, more of the ground off to the sides of the antenna is illuminated. In some of the models discussed the size of the refracted/transmitted GPR beam at a depth of 1 m might be as large as several meters.

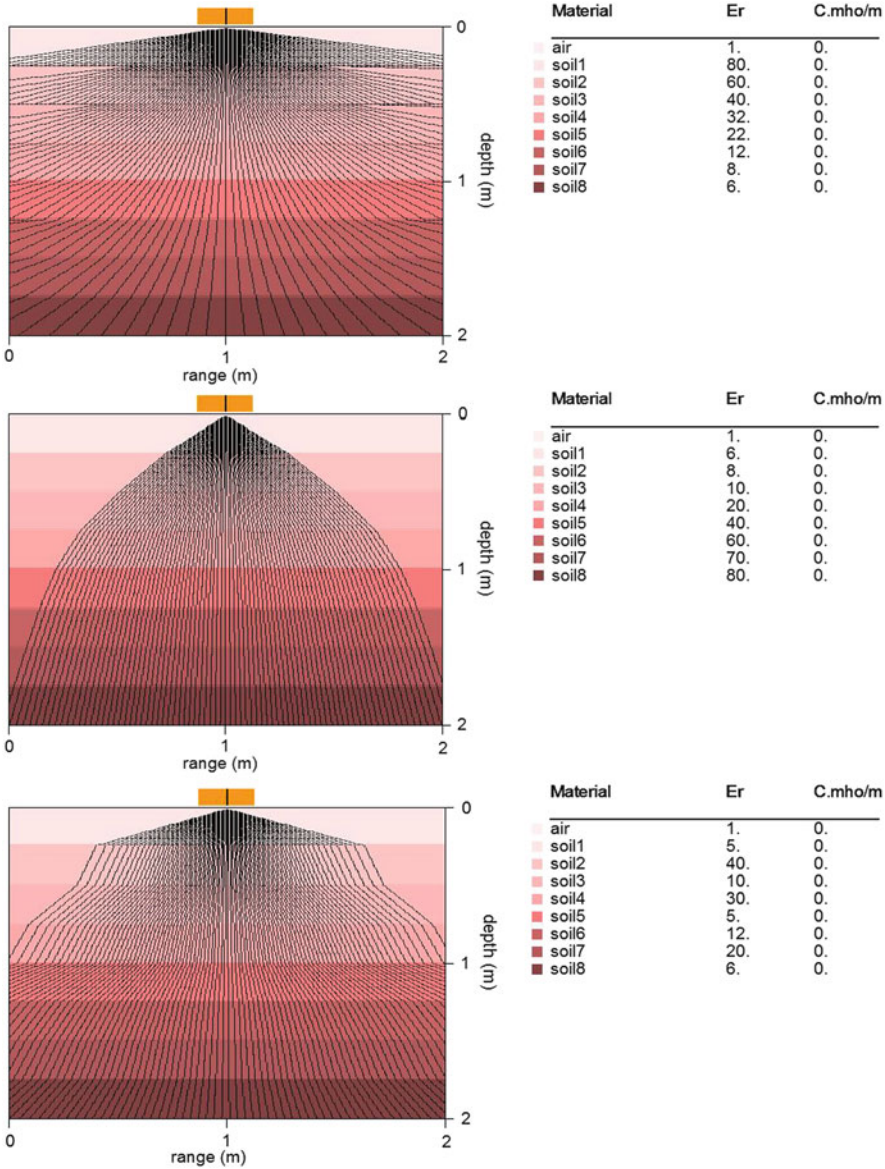
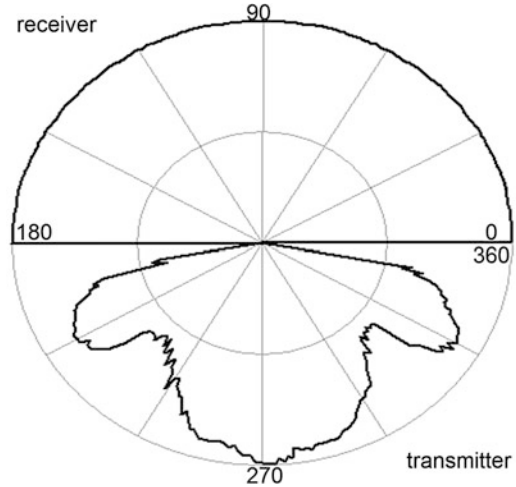


Fig. 2.3 Three idealized subsurface structures where the dielectric of the material is (a) increasing with depth (*top diagram*), (b) where the dielectric of the materials is decreasing with depth (*middle diagram*), and (c) a layered earth with random dielectric values. The *top diagram* shows the beam broadening and the *middle diagram* shows beam narrowing as the dielectric increases (velocity decreases with depth). The idealized earth model in *bottom diagram* shows a combination of varying dielectrics with low/high velocity layers. In this case, the beam can broaden or narrow across different boundaries

Fig. 2.4 An idealized directional response of a bow-tie antenna. The transmitted response has side lobes near 60°. The “bumpiness” is artificially generated to indicate that real antenna are rarely perfectly symmetric in the transmitted beam response. In our simulator we will assume for simplicity that the receiving antenna records equally in all directions and we are just considering differences in the transmit beam



The beams width can ultimately place an error bar of a similar magnitude on the location of the (raw-unprocessed) reflections recorded back to the antenna.

In the case when the dielectric is increasing with depth – velocity getting slower deeper in the subsurface, the beam of the GPR antenna will be focused – refracted downward (Fig. 2.3 middle diagram). This is actually the desired effect one would always wish for in GPR surveying – to have a narrow beam transmitted into the ground with less illumination off to the sides of the antenna. Of course a real earth model will have a much more complicated refraction pattern where waves will refract downward and then change to refracting away from the vertical with multiple and varying combinations (bottom diagram in Fig. 2.3). The GPR transmitted beam in the ground in this instance can widen or get narrower at varying boundaries in the earth.

The refraction of the radar waves is important since our simulator needs to trace the exact path each of the rays of energy emanating from the idealized antenna travel in order to see if the ultimate path gets reflected back to the antenna.

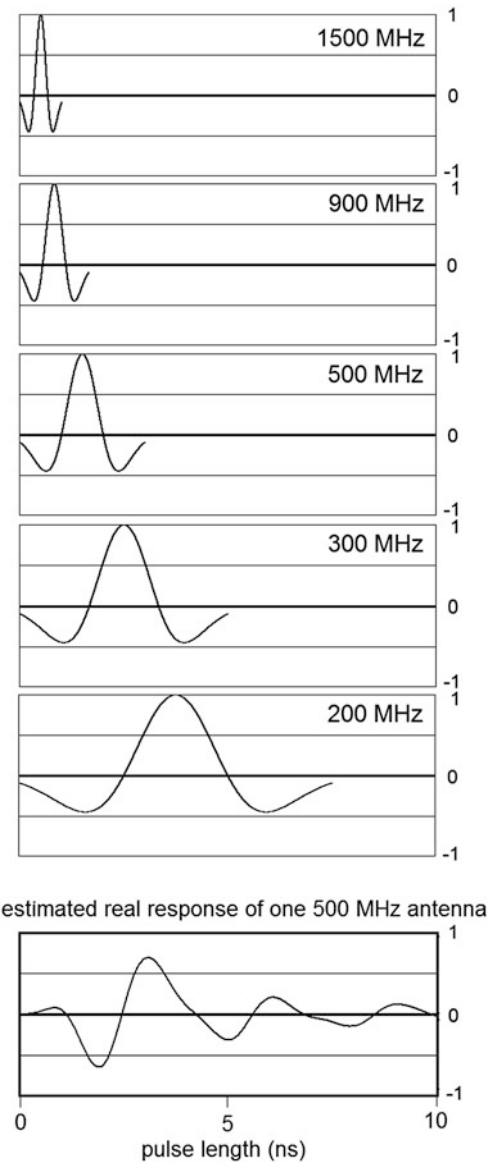
(It should be noted that there is a critical angle – Brewster’s angle – after which no energy will be transmitted into the deeper material. Past the Brewster angle, evanescent waves exist (Annan 2009)).

2.5 Attenuation

In order to simulate microwaves propagation we also need to know how GPR waves will attenuate as they travel in the ground. The attenuation is primarily controlled by the conductivity. The higher the conductivity of the material, the faster the wave will dissipate into the ground. The formula to describe the attenuation

$$a = \omega \sqrt{\frac{1}{2} \mu \epsilon'} \left[\sqrt{(1 + \tan^2 \delta)} - 1 \right] \quad (2.12)$$

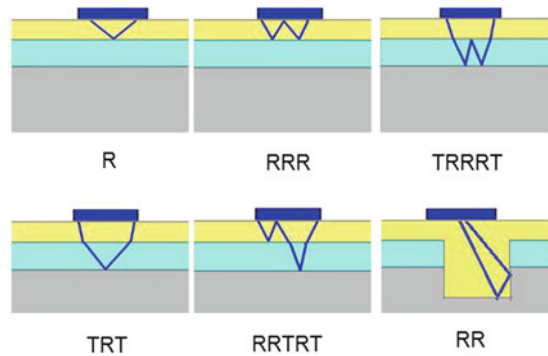
Fig. 2.5 An example of a damped sinusoidal response for varying frequencies and a comparison with an estimated real response of one 500 MHz antenna



is related to the loss tangent (shown in the Earth model section) of the material which is a combination of the dielectric and conductivity. Microwaves traveling through a material will exponentially decay as $e^{-\alpha}$. The larger the attenuation factor the quicker the microwave pulse will dissipate in the material.

Table 2.1 lists the attenuation of different materials provided for a nominal microwave frequency of 400 MHz. The attenuation factor is often listed as the decrement of a wave in traveling 1 m. For instance in the table for idealized air where there is no

Fig. 2.6 Examples of several different type of raypaths that can be recorded on a three layer earth. *R*, *TRT*, *RRR*, *RRTRT*, *TRRRT*, *RR* are possible energy paths that microwave energy can travel



conductivity, the attenuation in 1 m of travel is 0 – the microwave does not change or lose energy. For a clayey soil for example (dielectric = 15, conductivity = .05 mho/m), the attenuation of the wave will be 0.09 ($\exp(-2.42)$) of the initial amplitude after traveling 1 m. The microwave pulse will be less than 10 % of initial amplitude. If the wave travels another meter, the wave will be 0.0081 (0.09×0.09) of its initial amplitude or less than 1 % of its original amplitude. Thus clayey soils highly attenuate microwaves. On the other hand, some completely (dry) clayey soils that have lower conductivities than that described in this example may not attenuate microwaves dramatically. Just a little inclusion of water however, dramatically changes the conductivity/attenuation of a material. Most materials are dramatically changed by the insertion of water and any increase will always make the material attenuate microwaves faster.

In our simulator, the change in amplitude of the wave caused by conductive dissipation is monitored and integrated along the path of the wave. The initial wave can undergo extensive amplitude changes along the raypath caused by reflection/transmission at model boundaries, but the wave will also be attenuated continuously within a homogenous material as it travels. Should the wave return to the receiving antenna, the final amplitude from reflection/transmission changes as well as from attenuation along the raypath will be recorded. Whether or not the final amplitude recorded is significant or not will be shown in the synthetic radargrams which will add up all the energies reflected back to the receiving antenna.

2.6 Antenna Beam

The refraction of radar waves is dependent upon the initial angles that are transmitted into the ground. The antenna beam – or directional response function – determines the amount of energy that is radiated in each direction from the antenna. All antennas normally radiate energy in a 3D cone of varying broad or narrow angles with complicated patterns of amplitude that vary in different azimuthal angles (Yarovoy et al. 2007; Daniels 2009). In archaeological applications the most widely used antenna is the bow-tie antenna which have a main lobe and

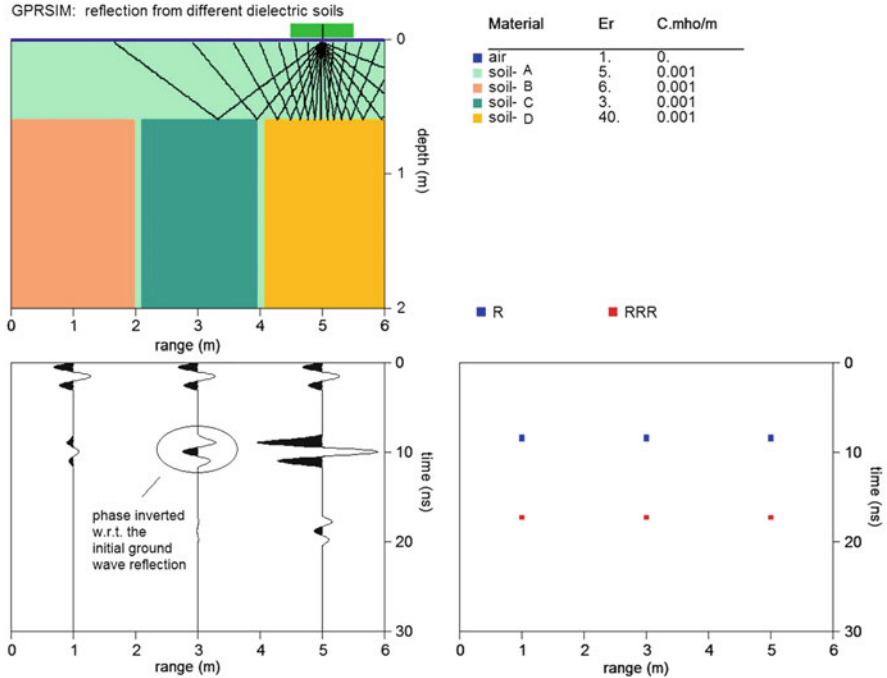


Fig. 2.7 In this GPR simulation the reflection off of three different materials with varying dielectric contrast embedded the matrix soil $\epsilon_r = 5$ is shown. The first reflection has a dielectric $\epsilon_r = 6$ which is very close to the background soil and thus the reflection is weak since the contrast is small between the soils. In the *middle* soil $\epsilon_r = 3$ the reflection is larger since the contrast between the two materials is slightly larger. Note that the middle reflection pulse appears inverted w.r.t. the ground wave. The reflection off the third soil is largest since the dielectric $\epsilon_r = 40$ is much different than the background soil. RRR wave energy has a travel path in the ground, that initially reflects off an object, returns to the top air-ground surface and reflects there, then travels downward again and reflects a third time to be recorded back to the receiving antenna and is included. The multiple reflection RRR wave shows significant energy being returned to the antenna when the contrast is highest for the third material; and completely negligible for the first material which has low contrast with the surrounding soil. (Some range gain have been applied to the synthetic pulses). Direct multiples from the surface usually have twice the travel time of the primary reflecting energy

sidelobes. A typical radar pattern for parallel bowtie antennas can look something like that shown in Fig. 2.4:

The sidelobes of typical bow-tie antenna are close to 60° off the vertical (Daniels 2009). This pattern shown is a simple 2D slice through the radar beam. The beam response perpendicular to the co-dipoles transmitter and receiver antenna is usually much narrower and the main beam is directed more vertical with lower transmission

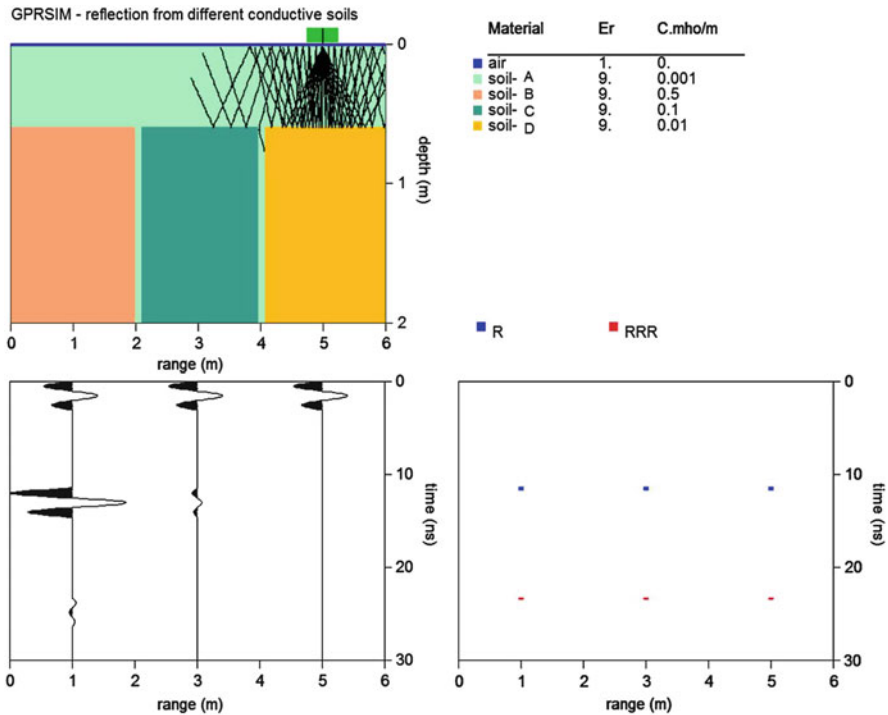


Fig. 2.8 In this example the importance of conductivity on the reflected field strength is simulated. To see the effects of just conductivity, the dielectric of all the materials are kept constant and just the conductivity is allowed to vary. For the higher conductive material (0.5 mho/m) the reflection is much larger than materials which have conductivities closer to the background material. Conductivity contrasts – not just dielectric – controls the reflected/transmitted wave amplitudes. Multiple reflections from just conductive differences can also generate significant returned energies when the contrast between materials is high enough. (In the figure the RRR multiple wave reflections are indicated on the third material)

strengths off to the sides. We only consider the parallel direction of the antenna as that is the most common orientation used in archaeological surveying. It should be noted that broadside orientation of the antenna could affect detectability of structures since the beam is typically narrower and weaker (Leckebusch 2011). Since our simulator is a 2D simulator we will just be considering the 2D pattern of the antenna. For the simulations we are also ignoring unshielded effects of the antenna since there are in fact back lobe responses which become more prominent with lower frequency antenna. Unshielded antenna that radiate and receive over 360° can be implemented in borehole simulations, but for the sake of most GPR applications for archaeology our simulated antenna are assumed to be perfectly shielded as we design them and radiate over only a hemisphere in the ground. The radiation pattern is also altered by the electrical properties of the surface material and the height of the antenna above the ground (Annan 2009). The exact pattern of

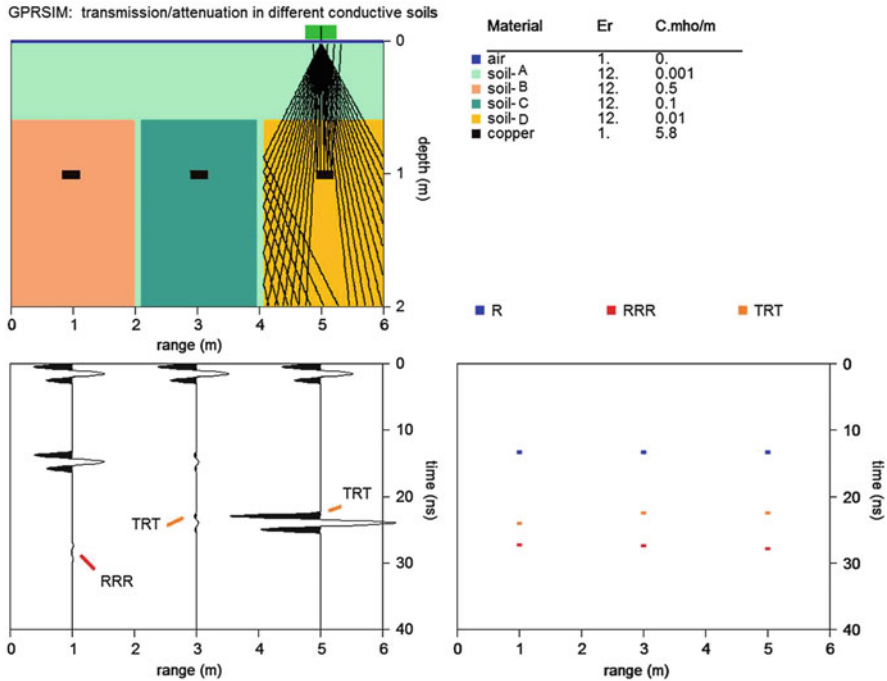


Fig. 2.9 Reflections and transmission partitioning at an interface dictate whether sufficient energy is available to detect features just below the interfaces. In this simulation, a copper box is buried in materials with conductivities ranging from 0.5, 0.1 and 0.01 mho/m. The dielectric of all materials is kept constant at $\epsilon_r = 12$. In the first material, the contrast between the background and the soil is so large that most of the energy is reflected at the top interface – no measurable reflected energy is observed that gets transmitted across the boundary to detect the copper box. The multiple reflection at depth, the RRR wave is detected however. In the third material, most of the energy gets transmitted across the boundary so that the reflection from the copper box is strong. Just as the R wave is not seen since the contrast is negligible between the background material and the third material, the RRR wave would be essentially nonexistent in terms of signal strength. The middle model shows a transitional electrical contrast state for comparison. Here the reflection from the top of the second material and the reflection from the copper are detected although relatively weak. The conductivity which is responsible for the contrast in the materials is also playing a part in the attenuation as the wave travels. The higher the conductivity in the material the faster the wave will attenuate

any manufactured antenna is really difficult to know precisely. Slight infinitesimal changes in the antenna surfaces can generate different patterns between what are “identically” manufactured antennas. In our simulator however, we will assume that the transmitted energy will follow the typical GPR beam as shown in Fig. 2.4. We will also assume that the antenna receiver can record waves equally in all directions without loss of recording energy in any given direction. This functionality is idealized by the blue receiver response which is set to 1 in all directions for simplicity. In reality, it is difficult to independently measure the receiving response

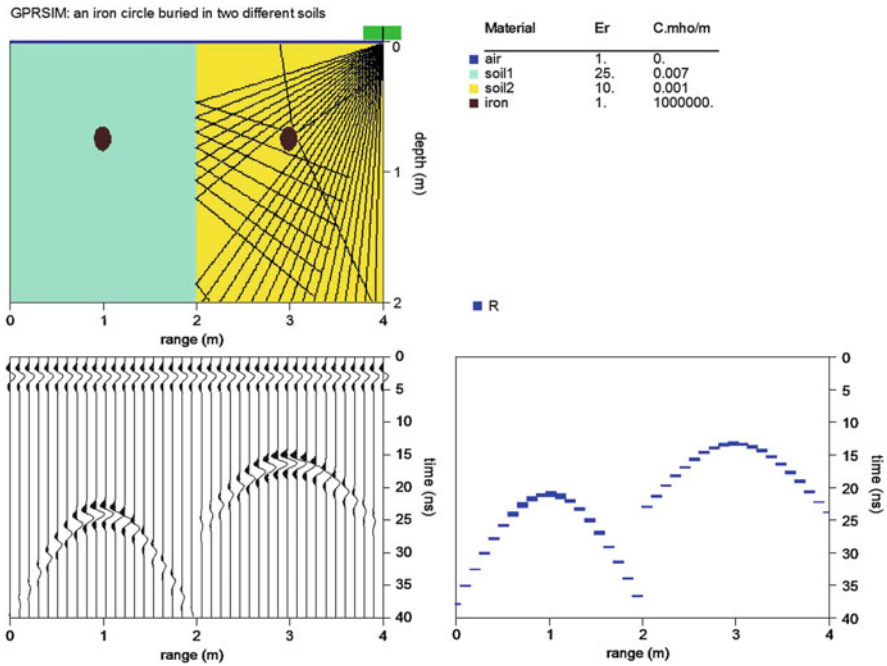


Fig. 2.10 A classic simulation to help assist beginners with the GPR technology, is to see the impact of varying matrix materials on an identical round object that is buried at the same depth in two different dielectric materials. On the *left hand side*, the *light green* material has an $Er = 25$ corresponding to a velocity of 6 cm/ns and the *yellow* material is $Er = 9$ which has a faster velocity of 9 cm/ns. The net effect of surveying with broad beam antenna is to generate a recorded hyperbolic reflection from each of the buried circular objects. The hyperbolic reflection from the object buried in the slow material – takes overall longer travel times for the reflections to be recorded back to the receiving antenna the overall reflections. The reflections from the circular object in the faster material take less travel time to return to the receiver. The hyperbola shape and narrowness is a function of the velocity of the material the object is embedded in. With software one can fit a hyperbola to the observed hyperbolas and discover the velocity of the matrix material the round target is buried in. (The complete mathematical description of the GPR hyperbola is presented in the section for migration in Chap. 3)

separate from the transmission response since they are convolved together in the final recorded measurement.

The antenna beam in the simulator is sampled at varying increments in order to send rays of energy into the ground at very small angles. In some of the simulations the density of rays along the beam can be sent into the ground at coarse 1° angular intervals or more. However, in some models because of the small scale structures to be imaged and the deeper depths to target structures, $1/10$ of a degree intervals or even smaller are used to ensure that small scale structures buried deep in the ground are properly sampled and bombarded with rays from the simulator.

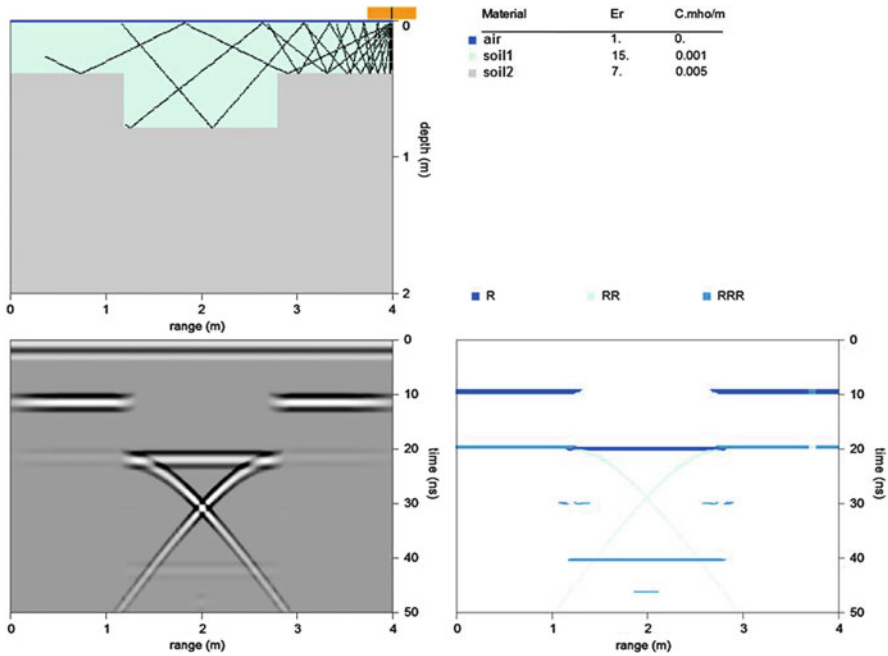


Fig. 2.11 A square trench has a distinctive radar pattern. The RR wave for this model represents a double reflection that bounces off one side of the trench and the trench floor and is then recorded. Two apparent half hyperbolas can be seen in the center of the trench. One of the pitfalls to avoid making is to interpret these reflections as resulting from several pipes round objects located near the corners of the trench on each side. The reflections are simply from multiple RR waves that are recorded. In this example, the depth to the top of the square trench on the sides is the same height of the trench floor below ground. What this translates into is the R wave from the bottom of the trench arrives at the same time as an RRR wave which is recordable but has lower reflections. Interpreting the RRR wave energy and the R wave from the bottom of the trench as being another continuous reflecting layer with variable reflection strength would be an incorrect interpretation

2.7 Antenna Pulse

With the antenna beam described, the simulator next requires the shape of the impulses being sent out of the antenna to be defined. GPR antenna send out a burst of microwave energy along the beam front that has an impulse response which when idealized resembles damped or Ricker wavelet sinusoids (Fig. 2.5). The real response of pulse transmitted from the antenna may show reverberations for several nanoseconds or pulse widths. Ideally, engineers would like to generate a pulse that is so narrow that the pulse might look like a simple spike and have no radiation of energy except vertically downward. With the current ground coupled antennas used today, a sharp pulse with a short duration cannot be realistically achieved (Daniels 2009). A typical transmitted pulse estimated for one GPR antenna with a central frequency of 500 MHz antenna is shown. The frequency often refers to the central

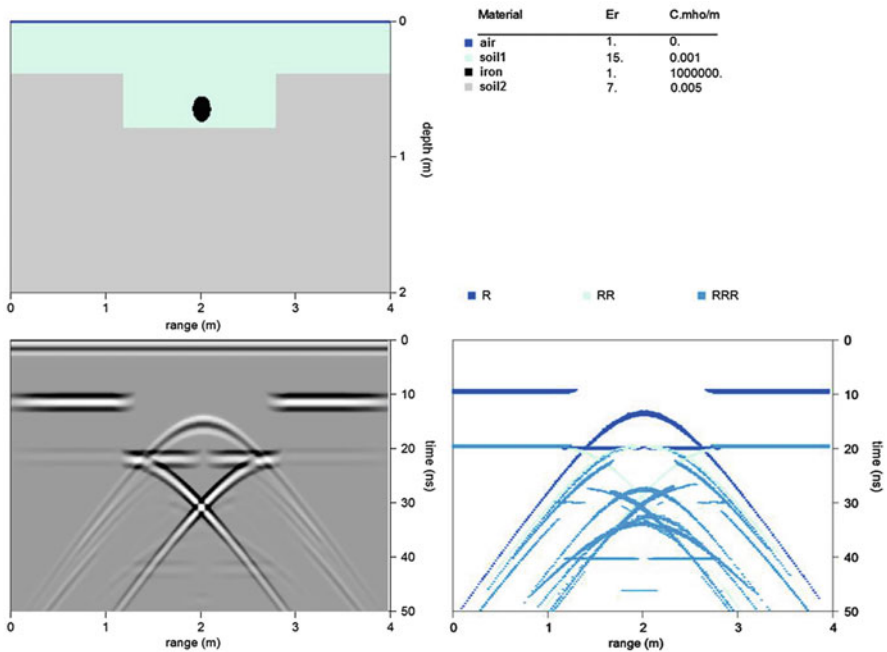


Fig. 2.12 A square trench with a pipe in it has a complicated radar pattern. The combination of RR and RRR waves that rick shays off the pipe or the walls of the trench and back off the pipe or the floors of the trench can produce many faint and measurable hyperbolic-like reflection legs. The half hyperbolic tails from the RR wave can give the false impression that other materials or pipes may be buried when in fact all the complicated recorded reflections are caused by multiples from the radar waves bouncing inside the trench. In sites where we have more homogenous structures and sharp boundaries, the above features can be seen in real recorded radargrams. However, as the boundaries are diffuse with less sharpness, the multiple reflections seen in the synthetic are less likely to be apparent

frequency band or the peak frequency of the antenna. The antenna usually have a wide band around the center frequency. The transmitted pulse can be estimated by measuring reflections from a perfect metallic object, however, this recorded response is just an estimate of the response. The recorded response is actually a combined response of the transmitted impulse which gets modified by the receiving antennas to give the final combined response. The receiving antenna may have directional recording responses which are not equal in all directions and not identical to the transmitter response.

In most of our simulations shown in his section for introducing GPR we will assume a simple damped sinusoidal response for the transmitted pulse coming out of our antenna, realizing that the true shape of transmitted pulse for any given antenna may not be so ideally designed. For some simulations in later sections where comparisons with real radargrams are modeled, estimated responses of the true transmitted response are employed.

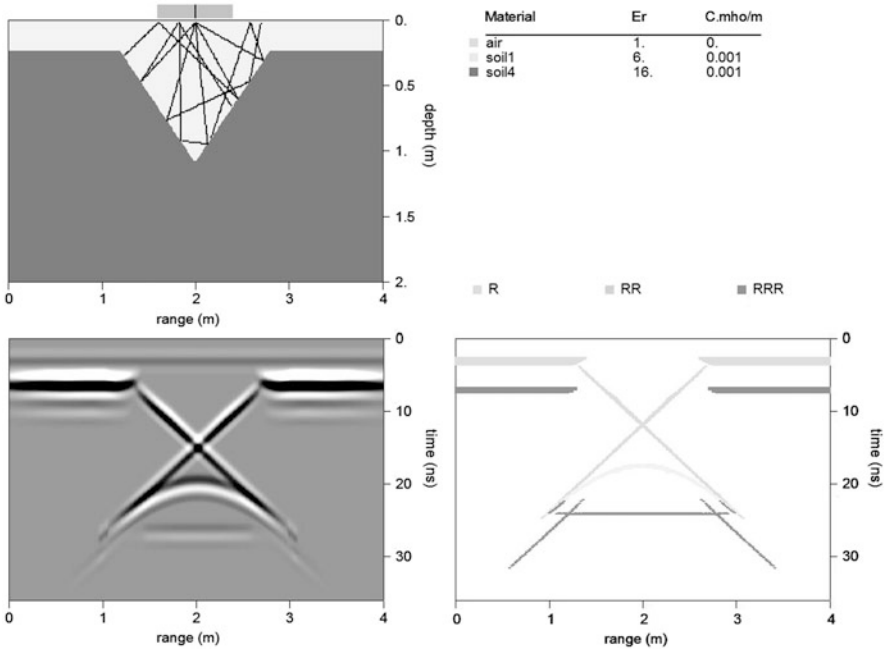


Fig. 2.13 A V-trench has a very distinct reflection pattern. The RR wave in this structure can generate a rounded reflection at the apparent center of the trench. Interpreters will often mistake this RR reflections as representing a pipe being located in the center of the trench. Another common interpretation pitfall is the improper identification of direct reflections legs on each side of the trench. The observed reflections from the R wave on each side of the trench center are actually coming from the opposite sides of the trench, e.g. energy that is recorded from the right side of the trench is only detected when the antenna is on the left side of the trench, and vice-versa. Another interesting reflection is the triple RRR wave which for a V-trench model can have a flat reflection multiple located near the apparent bottom of the trench (in this example near 22 ns). The actually pattern that is recorded from a V-trench is very sensitive to the depth of the trench as well as the narrowness. For narrower V-trench the RR reflection may not be recorded or will not generate a pseudo hyperbolic reflection in the center (see Goodman 1994)

2.8 Raypaths

Once the impulse response function is defined for the ground probing antenna, the next step is to determine what energy paths the transmitted wave through the model might take. Our simulator might be likened to a glorified “pinball machine” where we send in a ball into the game area with a certain speed and maybe angle, not knowing where the ultimate path of the pinball might travel. The same with the GPR model, rays are sent into the model at regular spaced intervals emanating from the antenna. Some of the rays will return and get recorded – where others will dissipate and travel to areas where they will never be recorded or heard from again. Examination of the model can usually tell us which are the primary energy paths. For instance a model with several layers, we can expect energy to travel similar to some of the paths shown in Fig. 2.6. Waves that reflect are defined as R and waves

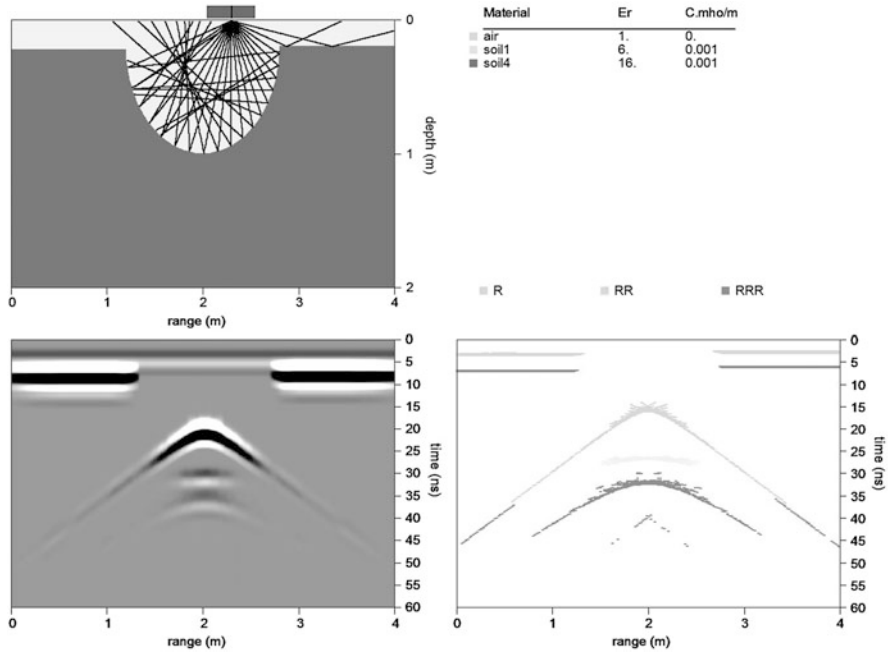


Fig. 2.14 A semi-circular trench extending to a depth of 1 m and with 1.6 m diameter can generate a reflection which is concave downward. This radar pattern is completely opposite of what one might expect. For the circular trench buried at deeper depths, the concave pattern will almost approach the look of a perfect hyperbola which can often mistakenly be interpreted as the reflection pattern due to a buried cylindrical object! The focusing of returned energy is dependent on the shape of the trench surface. In this case, a circular trench is modeled. A specially designed elliptical trench can wholly reverse the above observations – and shapes similar to what one might expect – such as a depression or concave up reflection can get recorded. The focusing or defocusing of GPR waves is very sensitive to small changes in the profile of the reflecting surface. The learning point here is that the shapes recorded on raw radargrams may have the complete opposite structure in the ground and the interpreter must be careful in translating what they observe to what they attribute the shape of candidate reflecting structure is

that transmit, reflect, and then transmit through a material to get recorded are defined as TRT for example. Waves that undergo multiple reflections, such as a wave that exits the antenna, reflects at depth, then rises to the surface and reflects off the air-ground interface, then goes back into the ground and reflects again before getting recorded is referred to as a RRR wave. A wave defined as an RR wave for instance, in a plane layer model will never return to the recording antenna and can be ignored. However, if there is a corner in the model like that shown on the *bottom right* diagram in Fig. 2.6 is present, then a RR wave traveling back to the receiving antenna is quite possible. There are an infinite number of possible trajectories and raypaths a wave might take, but usually only a few of the raypaths dominate the recorded energy coming back to the antenna.

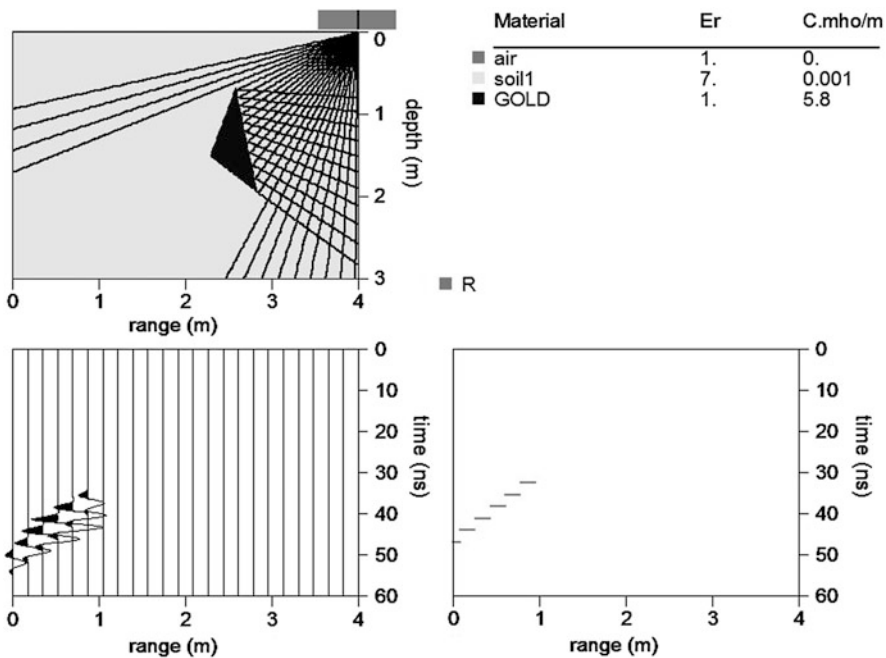


Fig. 2.15 To detect subsurface objects it is not just sufficient enough to have strong electrical contrast of the object with the surrounding soils to record reflections. The shape of the target is just as important. In this example a buried triangle with sharp edges causes the recording of reflections nearly 2 m from the actual location where it is buried. Directly above the triangle no reflected energy is recorded since a perfectly sharp edge of the triangle is modeled and does not have any significant flat surface that is oriented towards the antenna to send any rays back to the antenna. The back leg of the triangle does not reflect any energy back to the ground surface till at least the 4 m range. At larger ranges the right side of the triangle could reflect energy back to the direction of the antenna since the side is a few degrees less than vertical. However, the extra few meters for this geometry to become evident could also mean the wave will have attenuated by then, in addition to the travel time being outside the desired depth window chosen. The net effect is that no energy is recorded from the right side of the triangle for this simulation

Each time the ray reflects at some boundary, the amount of energy reflected is monitored for that ray (using Eq. 2.4). The attenuation as the ray travels is also continually updated as the ray travels through cells in the digitized grid (using Eq. 2.12). If the ray is required to undergo a transmission across a boundary, the amount of energy in the transmitted wave can be calculated (using Eq. 2.8) as well as the new angle of refraction that it will travel at in the new material (is found from Snell’s law – Eq. 2.11). The transmitted wave energy is continually monitored for the ray as well as the attenuation in the new material that the ray is traveling in. Should the ray make it back to the receiving antenna, the final energy in the recorded pulse is added up with all the other rays that are recorded. Many of the rays may arrive at different times and all will usually have different amplitude and different signs – +/– depending on whether the rays reflected off faster velocity

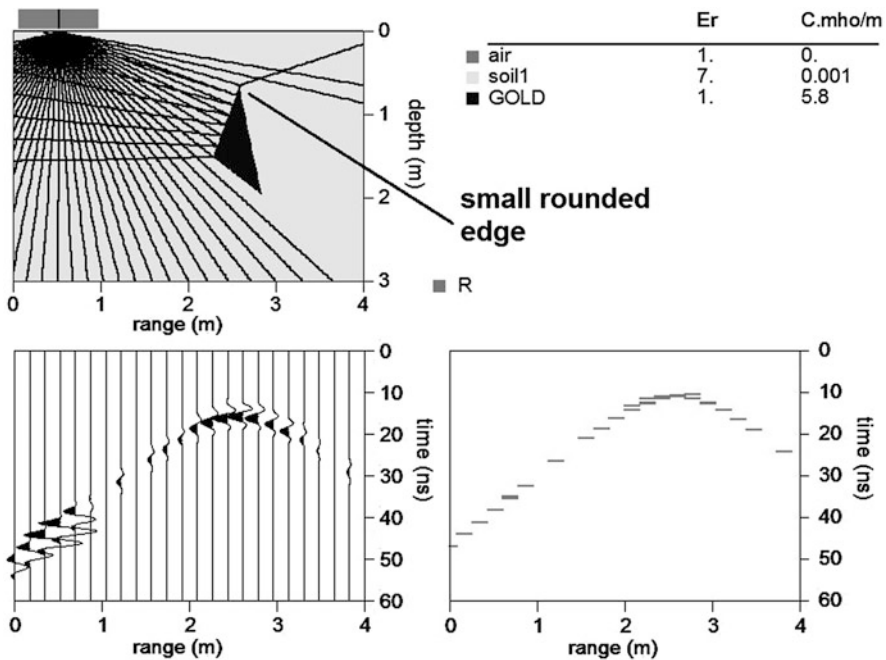


Fig. 2.16 The perfect triangle simulation shown previously indicates that no energy is recorded directly above the triangle since the super sharp edges have no flat or rounded portions too reflect any energy back to the receiving antenna. However, in the case when an edge is slightly rounded, then significant energy can be recorded from the top of the triangle. In this example an imperfection on the top of the triangle is modeled as a small semi-circle 2 cm in diameter to simulate a rounded edge. This small rounded edge can cause significant energy to be reflected back to the receiving antenna. This model explains why one component of Stealthy technology is to build outside structures with flat surfaces and to connect the surfaces so that the edges are as sharp as possible – which limits the radar returns and to prevent detection

targets along the travel path. Each of these small impulses arriving back to the receiving antenna from the multitude of different raypaths are convolved with the impulse shape of the transmitted antenna to generate a synthetic radargram for the model. Convolution is a mathematical process for simply multiplying the final recorded reflection/transmitted/attenuated response with the impulse response function of the antenna, and then adding up all these contributions for all the different rays recorded into a single and final – synthetic pulse.

The major components in the simulator have been described. A program called GPRSIM Ground Penetrating Radar Simulation Software (Goodman et al. 2009; Goodman 1994) contains all the elements for performing basic GPR modeling. The software fundamentally uses ray tracing through user drawn models and does all the calculations to predict the reflected/transmitted/attenuated/refracted radar waves returning back to the simulated antenna. The software allows for customized designs of the GPR equipment such as antenna impulse response and directional

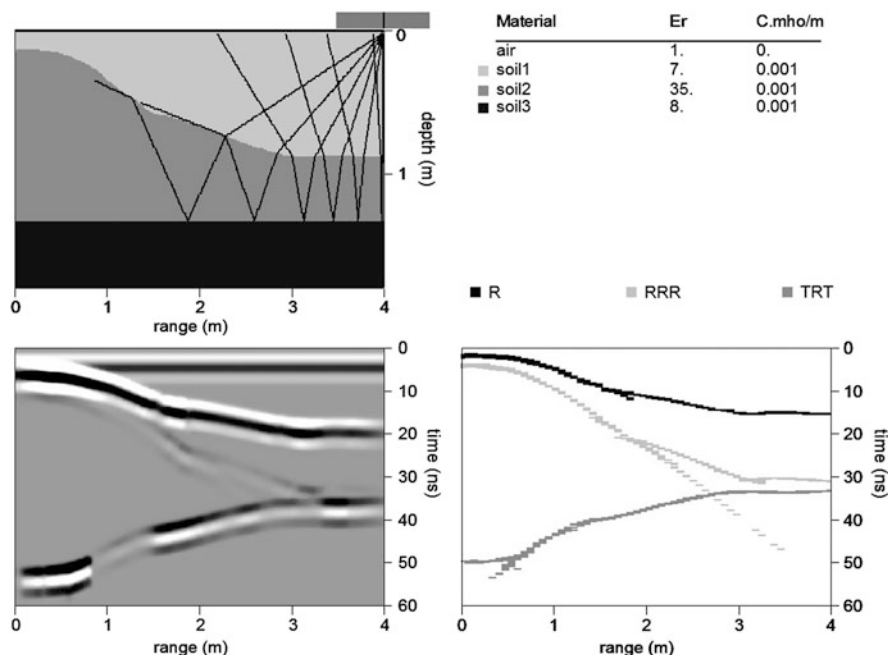


Fig. 2.17 Significant velocity changes between different materials can alter the shapes of radar structures from the “real” buried structures. In this example soil1 ($E_r = 7$, velocity 11.3 cm/ns) and soil2 ($E_r = 36$, velocity 5.1 cm/ns) have a velocity contrast of 6.2 cm/ns., with soil2 being much slower. The total travel time for a ray to reflect off the bottom layer takes progressively less time on the *right side* of the model than on the *left side* of the model. The reason being is that on the *left side* of the model soil1 is thinner and soil2 which is much slower in microwave velocity is thicker – causing the overall travel time to the bottom layer to take much more time. On the *right side* of the model, the faster material soil1 is thicker and there is less of the slower layer soil2 that the microwave must travel through. The travel time here is thus much faster for the TRT wave which reflects off the flat bottom layer. The net effect is to cause an upward warping of the flat layer on the *right hand side* of the model since overall faster materials exists here. This effect is referred to as a “velocity pull-up” in seismology. Flat reflectors at depth may appear as not being recorded at equal times due to possible strong velocity contrasts and variable layer thicknesses of the highly contrasted soils

beam response functions to be incorporated into the program and tailored specifically for different kinds of radar systems. Structural boundaries in the software are stored as splines, lines or the exact geometry of the feature. Bi-section method is used to further break down discovered cells with interfaces and find the exact reflection point of traveling rays. Even though a model might be digitized at 1 cm, further accuracy on the point of intersection in a grid cell is refined with bi-sectioning. In the simulation display the travel times of different raypaths are given as a separate graph from the synthetic radargram. The travel time plot is useful in showing the type of raypath recorded and the time that that a ray arrived back to the antenna. Although a ray may be recorded and identified on the travel time plot,

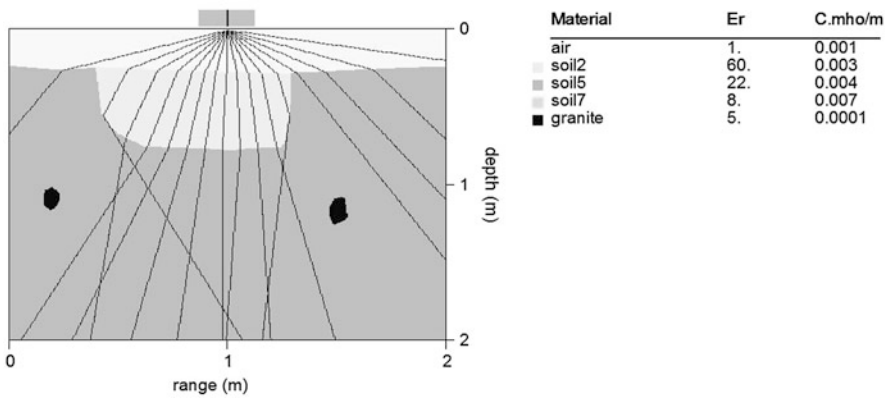


Fig. 2.18 An effect in GPR imaging that is rarely talked about but is very common in seismological studies are shadow zones. For certain subsurface structures with varying material velocities, GPR radar waves can refract in such a way that some areas of the subsurface are never sampled

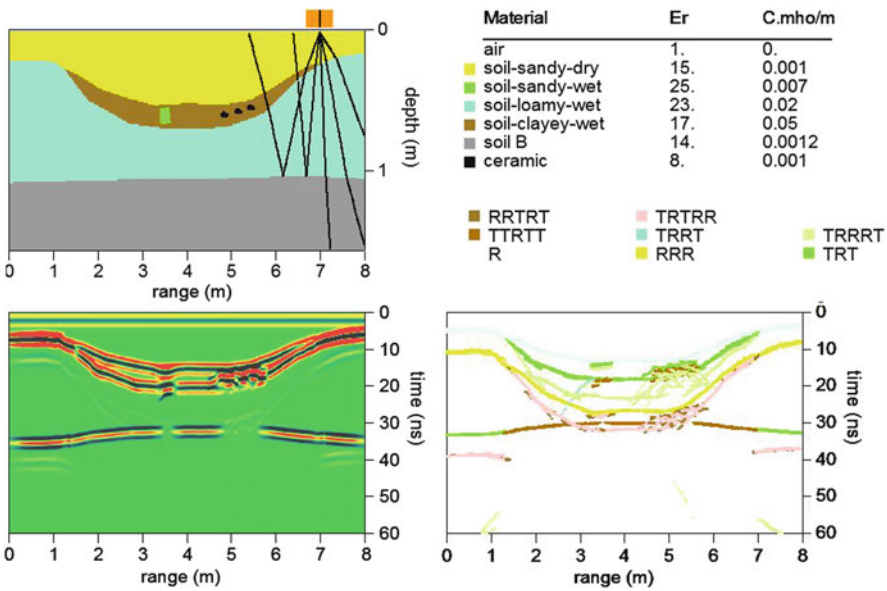


Fig. 2.19 Radargrams from pit dwellings often have recorded patterns which look closely like the real structures. In this example, a pit dwelling that has some structural materials embedded in the floor including pottery and a posthole is simulated. Differentiation of these smaller scale materials from the larger scale feature can sometimes be measured and defined on occasion in the field data, but more often than not these smaller features are not unequivocally interpretable. The recorded reflections can show several layers which may represent compacted floors and the reflections from the floor bottoms. Several multiples may also be apparent depending on the electrical contrasts between the soil materials. In general though, the large depression like feature indicative of a pit dwelling, can look very similar to the real structures buried in ground

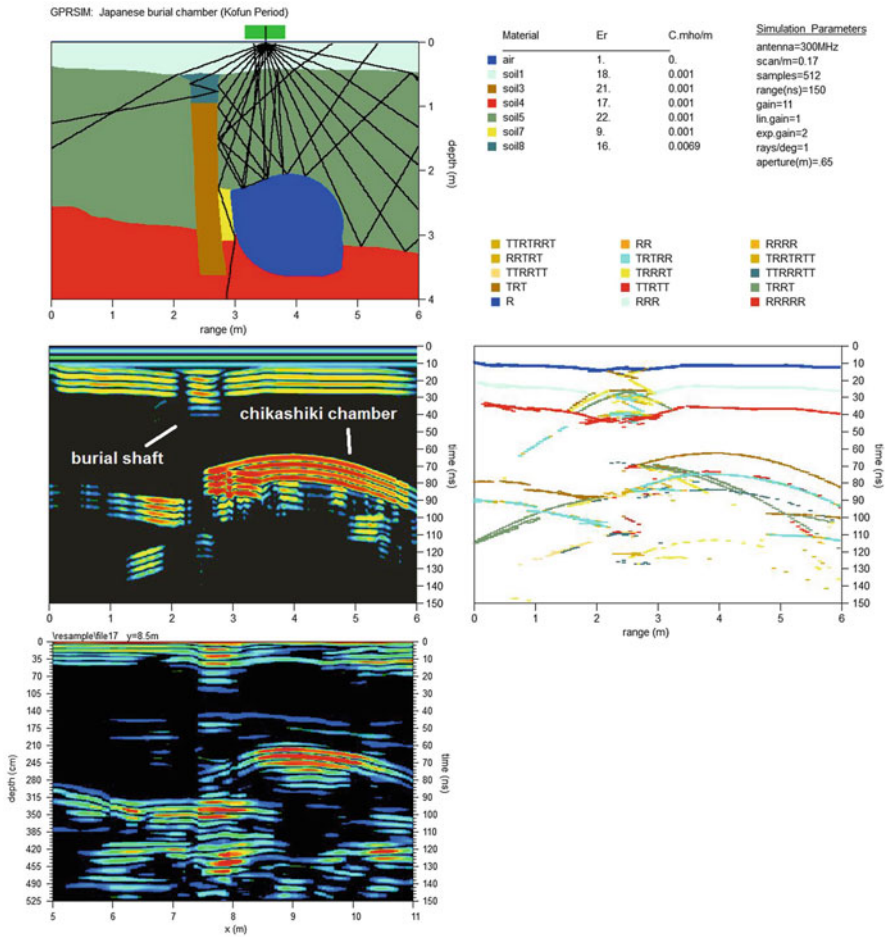


Fig. 2.20 A Japanese subterranean burial chamber (chikashiki) synthetic radargram is compared with a real radargram. In this burial construction design from the Kofun period (300–700 AD) a shaft was dug and a chamber excavated in hard-packed volcanic soils and is typical of structures found at the Saitobaru National Burial Mounds in Miyazaki Prefecture, Japan. The intact void chamber is recognized by a strong signal recorded from the roof. A small stone door might also be placed at the entrance after which the vertical shaft is backfilled with soil. Reflections from the shaft can often help to locate these features when the void chamber has collapsed and strong void reflections are no longer recorded from the main chamber structure. An example of a real radargram collected across the Sakamoto no Ue site in Saitobaru is shown. The reverberations recorded from the burial shaft and from the ceiling of the chikashiki chamber can be seen in the real radargram. In some instances, the rock door can be attempted to be modeled. From observations at similar sites it was found that multiple reflections between the shaft and chamber ceiling could produce strong reflections in the location where one would predict the stone door would be. The multiples could be falsely identified as resulting from a stone door (Edwards et al. 2000)

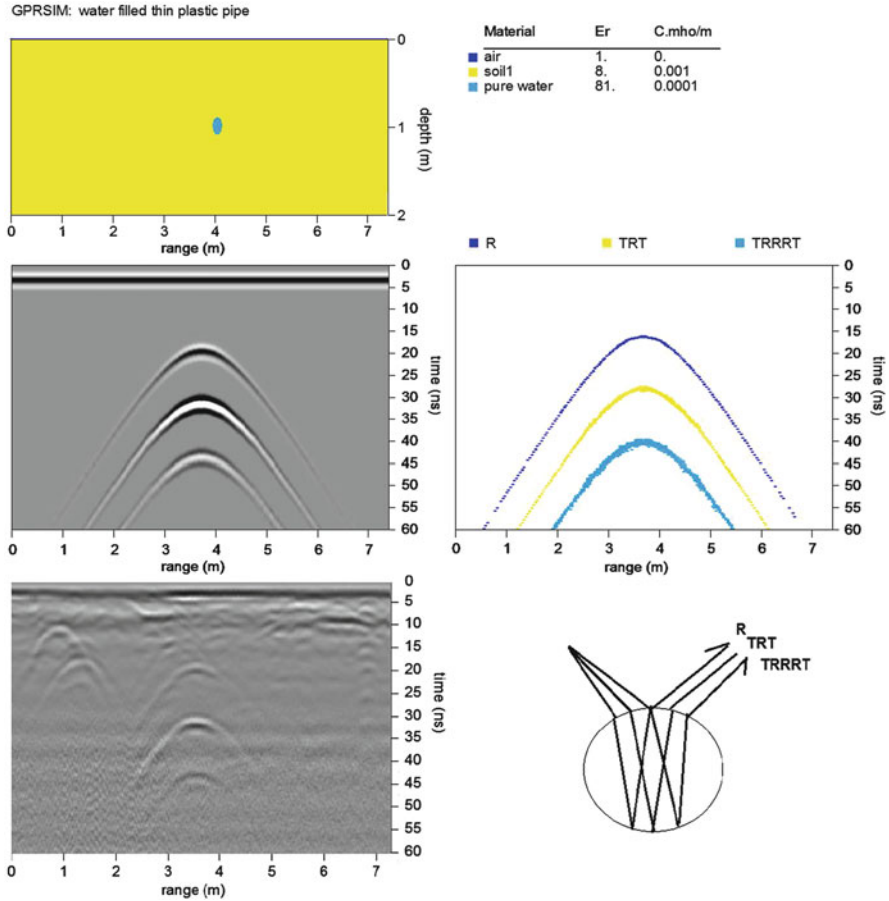


Fig. 2.21 In this example, a comparison of a real recorded radargram (*bottom diagram*) is compared with a simulated radargram. The model is a thin pipe buried in soil that is completely filled with water. As is often measured in real radargrams, several reflections that bounce from the bottom of the water filled pipe can be seen. The TRT wave and a wave that makes three reflections within the pipe, the TRRRT wave, are clearly recorded within the real radargram and also seen in the synthetic. The thickness of the pipe can also be estimated based on the time difference between the bounces if the dielectric of the internal fluid is known, e.g. pipe thickness = $v \frac{dt}{2}$, where dt is the time difference between the direct R and TRT wave that bounces off the bottom of the pipe. The site was a known location with a filled water pipe present (Courtesy of David Taylor, Spectrum Geophysics)

whether or not it is a significant component is manifested in the synthetic radargram; which has the returned amplitude convolved with the impulse response of the antenna.

The best way to see the net effects how GPR looks across structures, is to start out with simple features to see how the ground targets get translated and altered and eventually presented in the form of a raw radargram. Also, it is useful to look at

models with identical target features and shapes but that differ only by the electrical materials and to see how these changes can impact the recorded radar patterns. In Figure 2.7–2.21 examples of simulations across various models are shown. The simulations can help interpreters of radargrams to better understand the basic elements of GPR propagation, but to also comprehend why subsurface features do not translate directly to similar – recognizable structures on the raw radargrams. Comparisons with real recorded radargrams will be shown in several other chapters in this book including the chapter on historic cemeteries in North America and also a comparison with GPR across historic bridges in Spain. In addition, the use of signal processing on the synthetic radargrams to see how well certain filters operate will be shown in Chap. 3.

References

- Annan P (2009) Electromagnetic principles of ground penetrating radar. In: Jol HM (ed) *Ground penetrating radar: theory and applications*. Elsevier, pp 1–40. ISBN 978-0-444-53348-7
- Cassidy NJ (2009) Electrical and magnetic properties of rocks, soils and fluids. In: Jol HM (ed) *Ground penetrating radar: theory and applications*. Elsevier, Amsterdam, pp 41–72. ISBN 978-0-444-53348-7
- Daniels DJ (1996) *Surface-penetrating radar*. Short Run Press, Exeter. ISBN 0-85296-862-0
- Daniels DJ (2004) *Ground penetrating radar*. Institution of Engineering and Technology, London. ISBN 0-86341-360-9
- Daniels DJ (2009) Antennas. In: Jol HM (ed) *Ground penetrating radar: theory and applications*. Elsevier, pp 99–133. ISBN 978-0-444-53348-7
- Edwards W, Okita M, Goodman D (2000) Investigation of subterranean tomb in Miyazaki, Japan. *Archaeol Prospect* 7(4):215–224
- Giannopoulos A (2005) Modelling ground penetrating radar by GPRMAX. *Construct Build Mater* 19(10):755–762
- Goodman D (1994) Ground-penetrating radar simulation in engineering and archaeology. *Geophysics* 59:224–232
- Goodman D, Piro S, Schneider K, Nishimura Y, Hongo H, Higashi N, Steinberg J, Damiata B (2009) GPR archaeometry. In: Jol H (ed) *GPR theory and applications*. Elsevier, pp 479–508. ISBN 978-0-444-53348-7
- Leckebusch J (2011) Problems and solutions with GPR interpretation: depolarization and GPR data continuity. *Archaeol Prospect* 18(4):303–308
- Powers MH, Olhoeft GR (1995) GPRMODV2: one-dimensional full waveform forward modeling of dispersive ground penetrating radar data version 2. U.S. Geological Survey, Open file report, pp 95–58
- Ulriksen CPF (1982) Application of impulse radar to civil engineering. Ph.D. dissertation. Department of Engineering Geology, Lund University, Sweden
- Yarovoy A, Qiu W, Yang B, Aubry PJ (2007) Reconstruction of the field radiated by GPR antenna into ground. In: *Proceedings of the second European conference on antennas and propagation ELICAP*, pp 1–6



<http://www.springer.com/978-3-642-31856-6>

GPR Remote Sensing in Archaeology

Goodman, D.; Piro, S.

2013, XI, 233 p., Hardcover

ISBN: 978-3-642-31856-6